INTERNATIONAL SOCIETY FOR SOIL MECHANICS AND GEOTECHNICAL ENGINEERING



This paper was downloaded from the Online Library of the International Society for Soil Mechanics and Geotechnical Engineering (ISSMGE). The library is available here:

https://www.issmge.org/publications/online-library

This is an open-access database that archives thousands of papers published under the Auspices of the ISSMGE and maintained by the Innovation and Development Committee of ISSMGE.

Effect of cryogenic thermal exposure on geomechanical rock properties

M.Z. Rasheed & S. Khan

Curtin University, Perth, Western Australia

N. Tarom

Curtin University, Sarawak, Malaysia

ABSTRACT: The conducted study aims to investigate the effects of cryogenic thermal fracturing for well stimulation. Ten synthetic shale samples were produced and geomechanically tested under a confined and unconfined setup. A portion of the samples were exposed to dry ice while the remainder were tested without exposure. The results showed an overall weakening of the rock after being exposed to cryogenic temperatures. Ultimate Compressive Strength (UCS), Young's Modulus (E), and cohesion (c) decreased on average, whereas Poisson's Ratio (v) increased on average.

1 INTRODUCTION

With the rise of hydraulic fracturing came the increasing concern of the potential side effects of using a water based fracking fluid. One main side effect includes possible contamination of local water aquifers (Gray, Deutsch, & Marrero, 2017). The low viscosity fluidic nature of water allows it to become a conductive medium to transport chemicals into the aquifers. If implemented, waterless fracking technologies could reduce or completely eliminate this risk which would result in more widespread acceptance of fracturing techniques (Rassenfoss, 2013). The purpose of this study is to examine the effect of cryogenic temperatures on the geomechanical properties of synthetic rock samples.

Much like conventional fracking, cryogenic fracturing aims to enhance the flow of hydrocarbons through the reservoir and into the wellbore. The most common fluid base for cryogenic fracturing is carbon dioxide and nitrogen, which has been applied in the field to re-fracture originally stimulated wells (McDaniel, Grundmann, Kendrick, Wilson, & Jordan, 1998). This study aims to investigate the effects of dry ice as a cryogenic medium.

2 METHODOLOGY

2.1 Sample preparation

Shale samples composition was derived from a ternary diagram of four Barnett shale wells in the Unit

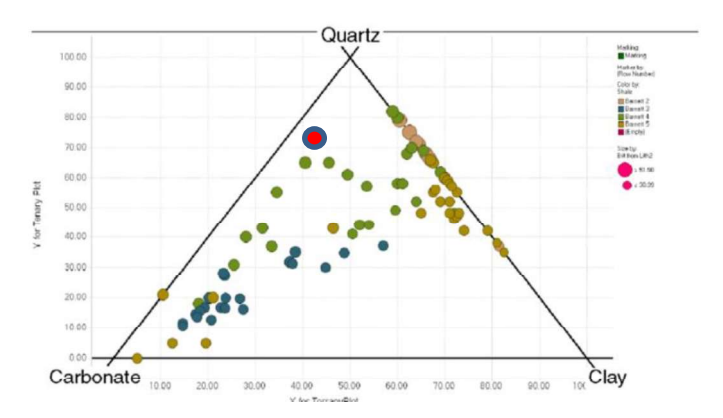


Figure 1. Composition of various shales in the Barnett (Rickman et. Al. 2008). Red circle indicates composition of samples in this research.

ed States (Rickman et. Al. 2008). The relevant composition used in the UCS testing is circled in red and represents 10% carbonate, 30% silica and 60% kaolinite clay. The ratio of water used to the weight of total mixture was 1.25.

With appropriate quantities measured, the dry ingredients were mixed together until a homogenous mixture was seen. The mixture was then filtered through a sift to remove any irregular sand particles (Figure 2).

Water was consistently added in a stage by stage basis, followed by mixing after each stage. Appropriate care was taken to ensure the right amount of water was measured such that the consistency of the slurry was neither too thick, nor too runny.

Packing this slurry into the cylindrical core moulds was the most crucial step in obtaining core samples that were free of imperfections. A core mould made from PVC pipe was used to replicate the shape of a

standard cylindrical plug of dimensions 78mm x 38mm (LxD), yielding a slenderness ratio of 2.05. Metal rings were fastened around the perimeter of the mould to prevent any excessive expansion of the slurry during the curing process. In addition to this, hydraulic oil was used to lubricate the inside of the mould to allow easy extraction post-curing.



Figure 2. Cement powder before and after the sifting process.

For the purposes of availability and ease of use, it was decided to use strain gauges for this research. As the sample can only be used once, it is especially important to ensure that the gauges are correctly working and that they have not been damaged through improper handling. Therefore, an ohmmeter was used to check the resistance of the gauges for each sample tested.

For a confined test the sample preparation procedure is slightly different when compared to a UCS test. A confined test requires thinner wires than the one used in the UCS test as the wires have to be nested within four grooves around the circumference of the platen. The sample with the appropriate wires attached to the strain gauges can then be taped to the bottom end platen (Figure 4). Similar to UCS testing, the resistivity of the confined test samples must also be confirmed.



Figure 3. UCS test sample with the strain gauges attached.

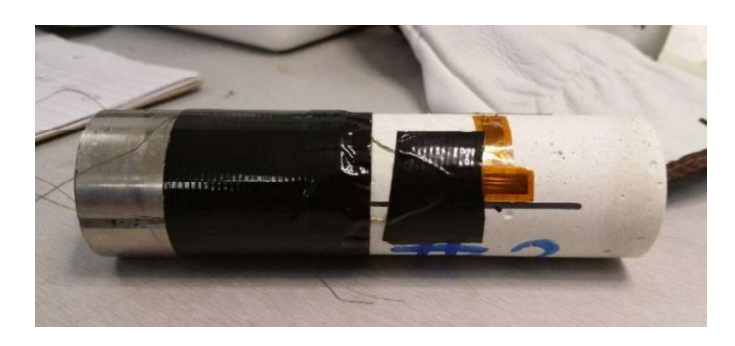


Figure 4. Sample preparation for a confined Hoek Cell test.

2.2 UCS testing

The samples were wired and placed under a RSM-100 jack using platens to reduce the distance the jack has to travel to reach the specimen. In addition to this, precise care was taken to ensure that the setup was straight between the top and bottom platens using an inclinometer. Axial and lateral strain was measured under a pump rate of 50 psi/min (345 kPa/min) until compressive failure.



Figure 5. Straight alignment from top platen to bottom platen to ensure accurate results (left) and same sample post failure (right)

2.3 Confined Hoek cell testing

Confined testing was done through the use of a hock cell. During the initial injection of the oil, one has to ensure that the cell is laid on its side to allow the oil to completely fill the empty space within the annulus of the internal sleeve and cell. Proper care has to be given to so that the sample sits directly in the centre of the cell and isn't closer towards the top or bottom end. Similar to the UCS test, an inclinometer was used to ensure the apparatus was straight from the bottom platen to the top (Figure 6, right).



Figure 6. Confined setup before applying a hydraulic load, an inclinometer was utilized to ensure proper alignment (right).

3 RESULTS

3.1 Geomechanical properties

The raw outputs given by LabView consist of time, confining stress, axial stress, axial strain and lateral strain. For this analysis, Young's modulus is the slope of the stress-strain curves between 20-50% of the peak UCS strength of the sample, before any non-linear deviation. The ultimate compressive strength (UCS) of the material can be read as the maximum value of axial stress.

After plotting lateral and axial strains against the axial stress, Poisson's ratio (v), can be determined using Equation 1 below. The results for the UCS tests and confined hoek cell tests can be summarized in Tables 1 through 3.

$$v = -\frac{\epsilon_{lateral}}{\epsilon_{axial}} \tag{1}$$

Table 1. Geomechanical properties of unconfined samples

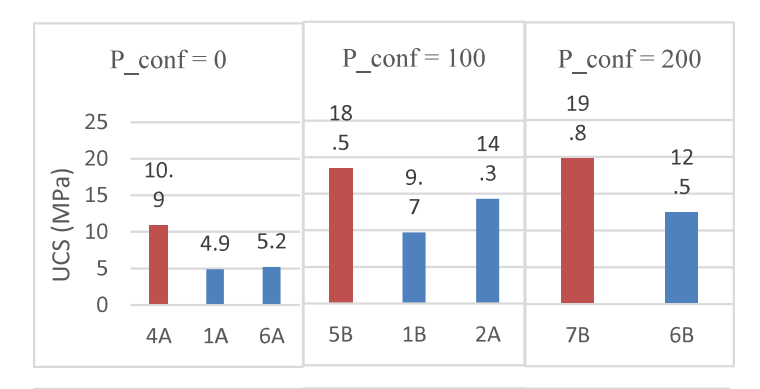
Sample	4A	1 A	6A
UCS (MPa)	10.9	4.9	5.2
E (GPa)	4.8	2.8	4.1
ν	0.12	0.16	0.23
σ_3	0	0	0

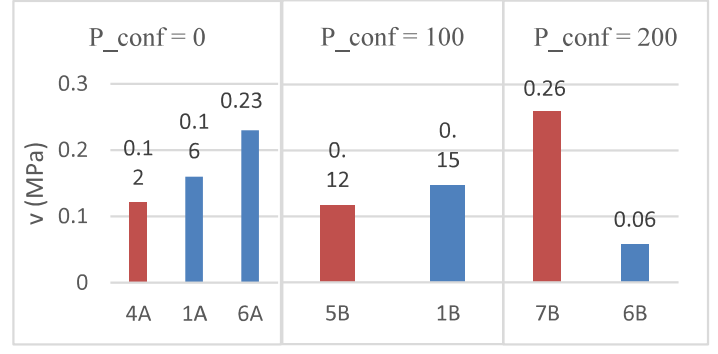
Table 2. Geomechanical properties of 100psi confined samples

	_	_
Sample	5B	2A
UCS (MPa)	18.5	14.3
E (GPa)	4.2	3.8
ν	0.12	0.15
σ_3	100	100

Table 3. Geomechanical properties of 200psi confined samples

Sample	7B	6B
UCS (MPa)	19.8	12.5
E (GPa)	12.5	2.7
ν	0.26	0.06
σ_3	200	200





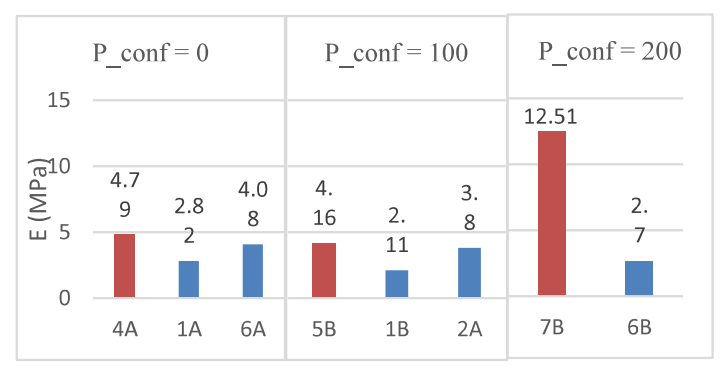


Figure 7. Geomechanical properties presented as bar graphs.

3.2 Mohr Coulomb model & stress-strain curves

A Mohr's circle was drawn to determine the failure envelope of the samples for easy comparison between the two cases of exposure and non-exposure. Stress strain curves for Samples 4A and 6A can also be seen in Figures 10 & 11 respectively.

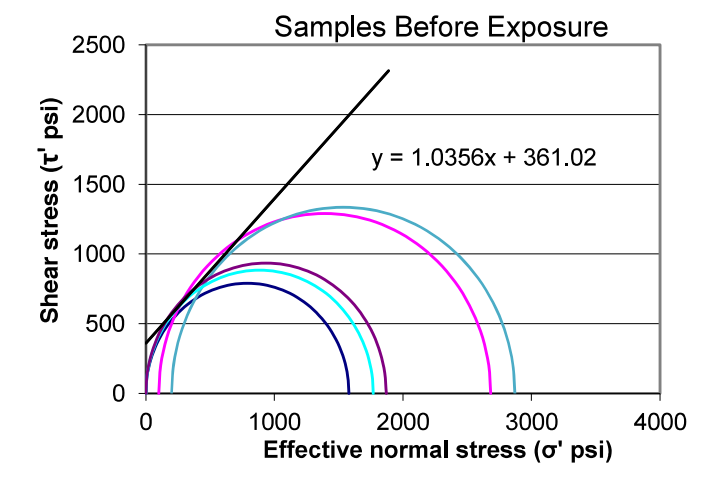


Figure 8. Mohr Coulomb model for samples before exposure.

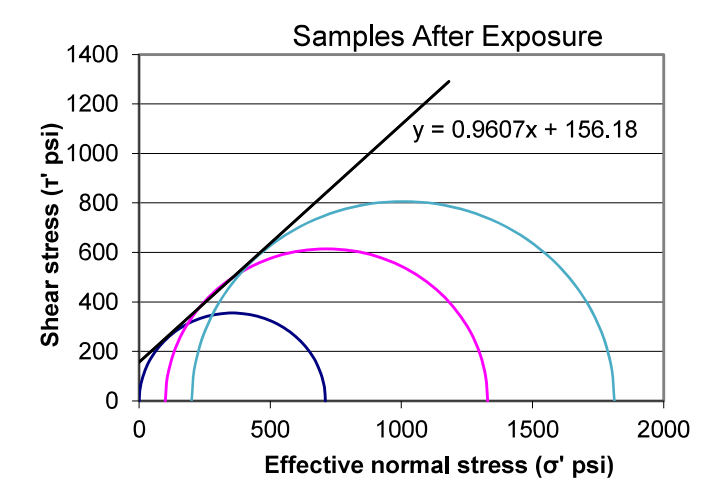


Figure 9. Mohr Coloumb model for samples after exposure.

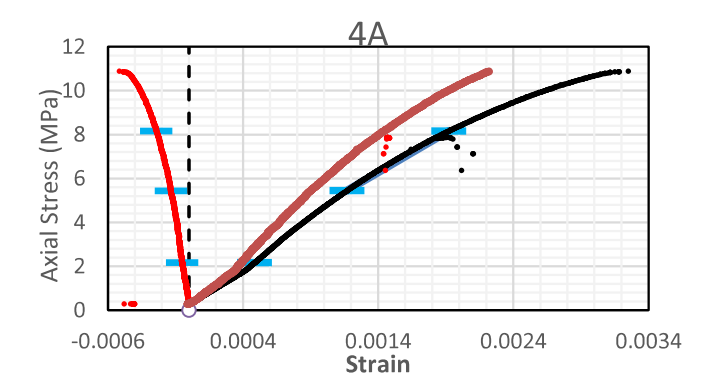


Figure 10. Stress-strain curve for an exposed sample.

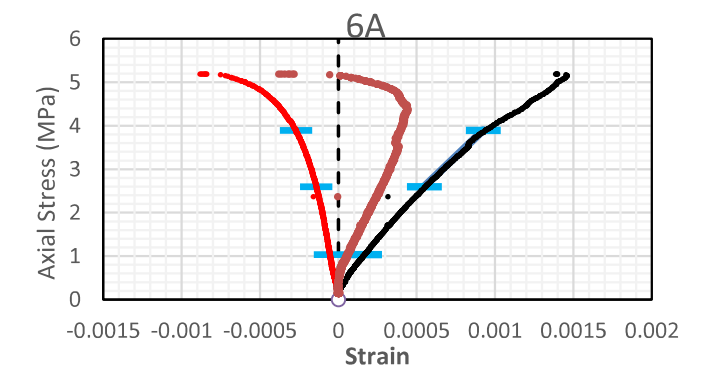


Figure 11. Stress-strain curve for an unexposed sample.

4 DISCUSSION

The decrease in the UCS and Young's Modulus in addition to the increase in Poisson's Ratio can be summarized in Tables 4 through 6. The change in UCS values demonstrate a correlation between exposure to dry ice with a decrease in the UCS of the synthetic rock sample.

These values are also quite consistent between tests, however the same cannot be said for Young's Modulus. There is a reasonable amount of discrepancy between values for Young's Modulus which could possibly be attributed to the sensitive nature of

the strain gauges measurements. This theory is reinforced by the fact that the UCS reading is independent of the strain and the fact that UCS results are consistent. The same discrepancies were also seen for Poisson's Ratio too. The maximum decrease for UCS and Young's Modulus and increase for Poisson's Ratio is 55, 78, and 48% respectively.

Table 4. UCS results summary.

Case (UCS)	Decrease (MPa)	Decrease
σ_3 (0 psi)	5.7 - 6	55 - 52%
σ_3 (100 psi)	9.3	50%
σ_3 (200 psi)	7.3	37%

Table 5. Young's Modulus results summary.

Case (E)	Decrease (GPa)	Decrease
$\overline{\sigma_3}$ (0 psi)	0.8 - 2	15 - 41%
σ_3 (100 psi)	0.4 - 2	9 - 49%
σ_3 (200 psi)	9.8	78%

Table 6. Poisson's Ratio results summary.

		· · · · · · · · · · · · · · · · · · ·
Case (v)	Increase (Fraction)	Decrease
σ_3 (0 psi) σ_3 (100 psi)	0.04 - 0.11 0.03	25 - 48% 20%
σ_3 (200 psi)	-0.2	- 77%

The discrepancies could be possibly explained as a result of experimental error. More specifically, the strain gauge applied to the sample being incorrectly placed, or being influenced by the confining pressure it was subjected to. Other possible reasons for this discrepancy include excessive glue being applied to the gauge, or improper handling which would alter the calibration of the gauge.

Furthermore, another source of error between UCS values could be credited to different loading rates between samples. According to Stowe (1969), a relatively static loading rate of 1 psi/sec (7 kPa/sec) correlates to a UCS value of 20,960 psi (145 MPa) while a rapid loading rate of 1.34E7 psi/s (92.4 GPa) correlates to a UCS value of 34,580 psi (238 MPa). However, it was concluded that this was not the case due to the similarity in the axial stress loading rates between each test (Figure 12).

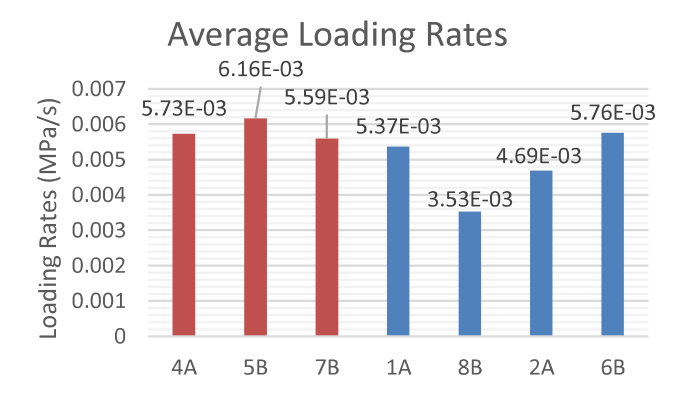


Figure 12. Average loading rates for all samples, fairly consistent loading rates can be seen.

In terms of the Mohr's Circles, the internal friction angle for both batches of samples remains unchanged, with an angle of 46° for the unexposed samples against an angle of 44° for the exposed samples. However, Figure 8 shows a cohesion of 2.5MPa for unexposed samples whereas Figure 9 shows a cohesion of 1.1MPa for exposed samples. This shows a significant decrease in the internal cohesion of the synthetic shale samples.

The results seem to be fairly consistent, with each test aligning similarly to other tests in the Mohr Coulomb failure envelope. This is further reinforced with a R^2 value of 0.889 for the unexposed samples and 0.995 for the exposed samples. Furthermore, calculated failure angle from the Mohr's Circle analysis was determined to be 67°, which aligns closely to the actual failure plane angle seen in Figure 13 below.



Figure 13. Failure plane for a sample, it can be seen that the angle of the plan with the horizontal is around 67° .

5 CONCLUSION

During this research multiple batches of core samples were prepared, with ten samples being used in the geomechanical testing. UCS testing was conducted on four samples and the remaining six samples were failed in a state of confinement using a Hoek Cell. For the confining tests, a 100 psi (689 kPa) and 200 psi (1379 kPa) confining pressure was used. Part of the sample preparation procedure included exposing six out of the four tested samples to a cryogenic medium, namely dry ice.

The calculated geomechanical parameters consist of UCS, Young's Modulus, and Poisson's ratio. UCS and Young's Modulus were seen to decrease with cryogenic exposure whereas Poisson's ratio increased. The degree to which UCS and Young's Modulus decreased were on average 48 and 30% respectively, while Poisson's ratio increased by 31% on average. The discrepancies in the results obtained could be possibly explained through experimental and human error.

Plotting the results obtained on a σ'_1 vs σ'_3 plot allowed for the internal friction angle and subsequently the angle of the failure plane to be determined as 67°. This value matched what was observed experimentally, as seen in Figure 13. Cohesion decreased in the linear Mohr-Coulomb from 2.5MPa to 1.1MPa.

REFERENCES

Gray, M., Deutsch, N., & Marrero, M. (2017). Current Regulatory Issues Regarding Hydraulic Fracturing, *held in* SPE: Society of Petroleum Engineers. http://dx.doi.org;10.2118/184859-MS

McDaniel, B. W., Grundmann, S. R., Kendrick, W. D., Wilson, D. R., & Jordan, S. W. (1997). Field Applications of Cryogenic Nitrogen as a Hydraulic Fracturing Fluid, *held in SPE: Society of Petroleum Engineers*. http://dx.doi.org:10.2118/38623-MS

Rassenfoss, S. (2013). In Search of the Waterless Fracture.http://dx.doi.org/10.2118/0613-0046-JPT

Rickman, R., Mullen, M. J., Petre, J. E., Grieser, W. V., & Kundert, D. (2008). A Practical Use of Shale Petrophysics for Stimulation Design Optimization: All Shale Plays Are Not Clones of the Barnett Shale, *held in SPE*: Society of Petroleum Engineers. http://dx.doi.org;10.2118/115258-MS

Stowe, R. (1969). Strength and Deformation Properties of Granite, Basalt, Limestone and Tuff at Various Loading Rates.

Retrieved from http://www.dtic.mil/dtic/tr/fulltext/u2/684358.pdf